International Journal of Pharmaceutics 376 (2009) 141–152

Contents lists available at ScienceDirect

International Journal of Pharmaceutics

journal homepage: www.elsevier.com/locate/ijpharm

Pharmaceutical Nanotechnology

Hyperbranched polysiloxysilane nanoparticles: Surface charge control of nonviral gene delivery vectors and nanoprobes

Won Jin Kim[a,b], Adela C. Bonoiu[a], Teruaki Hayakawa[c], Cheng Xia[c], Masa-aki Kakimoto[c], Haridas E. Pudavar[a], Kwang-Sup Lee[a,b,*], Paras N. Prasad[a,**]

[a] Institute for Lasers, Photonics, and Biophotonics, University at Buffalo, The State University of New York, Buffalo, NY 14260-3000, USA
[b] Department of Advanced Materials, Hannam University, Daejeon 305-811, Republic of Korea
[c] Department of Organic and Polymeric Materials, Tokyo Institute of Technology, Tokyo 152-8552, Japan

ARTICLE INFO

Article history:
Received 14 November 2008
Received in revised form 1 April 2009
Accepted 20 April 2009
Available online 3 May 2009

Keywords:
Polymer nanoparticle
Surface charge controllable nanoparticle
Nonviral gene delivery vector
Nanoprobe
Hyperbranched polysiloxysilane
Multi-photon cellular imaging

ABSTRACT

New hyperbranched polysiloxysilane (HBPS) materials containing terminal carboxylic acid and quaternary ammonium groups were designed and synthesized to obtain fluorescent-dye-encapsulated nanoparticles. These polymers exhibited desirable characteristics, including amphiphilicity for nanoparticle formation, and contained various terminal groups for surface-charge control on the nanoparticles or for further bioconjugation for targeted imaging. Nanoprobes composed of polysiloxysilane nanoparticles encapsulating two-photon dyes were also prepared for optical bioimaging with controlled surface charge density (zeta potential) for modulation of cellular uptake. Intracellular delivery of these structurally similar polysiloxysilane nanoparticles, with substantially different surface charges, was investigated using confocal and two-photon fluorescence microscopy as well as flow cytometry. Finally, the use of these nanoparticles as efficient gene delivery vectors was demonstrated by means of *in vitro* transfection study using β-galactosidase plasmid and pEGFP-N1 plasmid and the most efficient combination was obtained using HBPS-CN30:70.

© 2009 Elsevier B.V. All rights reserved.

1. Introduction

The use of nanoparticles as diagnostic probes and effective carrier vehicles in targeted therapy is gaining considerable interest. Recently, various organic, inorganic, and hybrid nanoparticle systems have been used for the nanocarriers and gene delivery vectors (Prasad, 2003). There have been several recent papers that have demonstrated the capability of tailored synthetic polymers such as dendrimers, block copolymers, hyperbranched polymers, and star polymers (Ramzi et al., 1997; Grohn et al., 2001; Tian et al., 2005; Pistel et al., 1999), consequently, to form nanoparticle as a nanocarrier. These polymeric approaches show enhanced therapeutic efficacy. Particularly, polymeric nanocarriers/vectors are typically prepared in the form of micellar nanoparticle because the molecular self-assembling architectures lead to the formation of the stable nanostructures which has two main components such as hydrophobic core and hydrophilic corona. The hydrophilic corona surrounding the core is known to play an important role in the cellular uptake, and hydrophobic core of micelles can act as the reservoir of drugs. It can be used in biological applications such as drug delivery vehicles, targeted cellular imaging probes, and gene delivery vectors (Benns et al., 2000; Midoux and Monsigny, 1999; Liu and Yao, 2002; Thanou et al., 2002; Wetering et al., 1999; Fischer et al., 1999; Marschall et al., 1999; Campeau et al., 2001). However, most of these nanocarrier systems exhibit only limited capability of controlling the surface charge of the nanoparticles to optimize cellular uptake and gene delivery efficiency. Furthermore, many of these carriers are often cytotoxic thus eliminating them from *in vivo* applications. To address some of these issues, we synthesized hyperbranched polysiloxysilane (HBPS) polymers containing amphiphilic components with different end groups. While the amphiphilicity of these polymers helps in the formation of aqueous nanoparticle dispersions, the combination of different functional end groups makes it possible to tailor the surface-charge distribution of the formed nanoparticles.

The novelty of these amphiphilic HBPS polymers lie in the fact that nanoparticles with different zeta (ζ) potential (surface charge density) can be easily tailored and functionalized. Indeed, the resulting hydrophobic cores found within the nanoparticles can be loaded with hydrophobic dye molecules or other hydrophobic drugs, which can be used as fluorescent probes in gene delivery or in drug delivery applications (Kim et al., 2002a,b, Midoux and Monsigny, 1999). Furthermore, HBPS polymers are composed of

* Corresponding author at: Hannam University, Daejeon 305-811, Republic of Korea. Tel.: +82 42 629 8857; fax: +82 420629 8854.
** Corresponding author at: University at Buffalo, SUNY, Buffalo, NY 14260-3000, USA. Tel.: +1 716 645 6800x2098; fax: +1 716 645 6945.
E-mail addresses: kslee@hnu.kr (K.-S. Lee), pnprasad@buffalo.edu (P.N. Prasad).

0378-5173/$ – see front matter © 2009 Elsevier B.V. All rights reserved.
doi:10.1016/j.ijpharm.2009.04.023

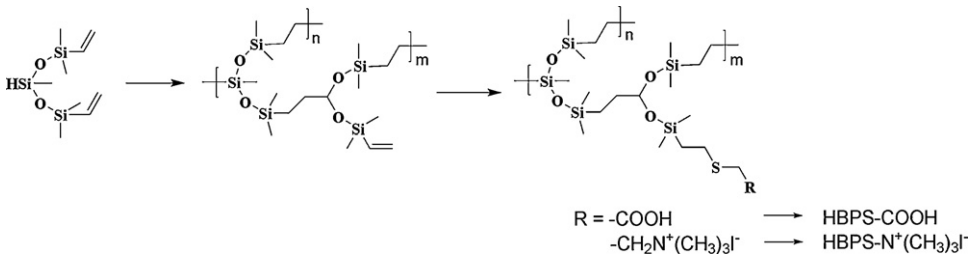

Scheme 1. Synthetic route for the hyperbranched polysiloxysilane derivatives.

amphiphilic components similar to linear polymer systems (Benns et al., 2000; Midoux and Monsigny, 1999; Liu and Yao, 2002; Thanou et al., 2002; Wetering et al., 1999), but they combine the advantages of numerous end groups with surface-charge controllability. This altered charge distribution surrounding the hydrophobic core of the nanoparticles provides the ability to optimize the uptake efficiency as well as the electrostatic condensation of DNA and its protection from enzymatic degradation. In addition, amphiphilic silicon-based polymers, such as HBPS, exhibit interesting properties that include biocompatibility, stable in an acidic environment, potential to easily functionalize SiH or Si-vinyl at the chain ends and unreacted sites for bioconjugation (Clarson and Semlyen, 1993; Das et al., 2002; Miravet and Frechet, 1998; Si et al., 2005; Park and Bae, 2003; Afanasyeva and Bruch, 1999). For all the above-mentioned reasons, the use of HBPS nanoparticles as a carrier of fluorescent probes, or as a nonviral vector, has tremendous potential.

The HBPS nanoparticles used in this study were prepared by self-assembly of the corresponding amphiphilic polymers in an aqueous environment (Graf et al., 1999). During the formation of these nanoparticles, other hydrophobic dyes/drugs could be encapsulated inside their hydrophobic cores. The hydrophilic character of polysiloxysilane was controlled by introducing various end groups, such as –COOH and $-N(CH_3)_3{}^+I^-$ (see Scheme 1). The presence of hydrophilic end groups in hydrophobic polysiloxysilane provides amphiphilicity to the polymers, thus allowing them to form nanoparticles in an aqueous environment (Savin et al., 2005). This simple modification of the molecular structure by changing the end groups may offer an opportunity to establish the effect of surface charge on the cellular uptake of various nanoparticle-based delivery vehicles. The synthetic polysiloxysilane compounds can be prepared in various electrostatic surface forms, which provide positive charges on the nanoparticle surfaces, attributed to the presence of quaternary ammonium groups, and negative charges resulting from the presence of carboxylic acid groups. Thus, the surface charges on these particles can be almost continuously tuned from highly negatively charged nanoparticles to highly positively charged nanoparticles by simply varying the composition of a mixture of the two polymers. This well-controlled surface charge density of nanoparticles is important for drug/fluorescent-probe carrier systems because many proteins, DNA, and cell-membrane surfaces are slightly anionic (Kass and Krafte, 1987). Our synthetic approach is a straightforward route for obtaining nanoparticles for cancer-cell probing or gene therapy. This method can be used for optically tracking the cellular pathway using fluorescent-dye-loaded nanoparticles or for gene delivery employing the nanoparticles as a nonviral vector.

Here we report the synthesis of HBPS, the preparation of nanoparticles using this HBPS, and the encapsulation of efficient two-photon absorbing dyes inside the nanoparticles as well as their surface modification. We also present the one- and two-photon optical characterization of the system and optical tracking of the cellular uptake of the prepared nanoparticles using confocal and two-photon microscopy. The use of the nanoparticles as nonviral vectors for gene delivery is also presented.

2. Materials and methods

2.1. Preparation of hyperbranched polysiloxysilane

2.1.1. Synthesis of 1,1,3,5,5-pentamethyl-1,5-divinyltrisiloxane (AB_2-type monomer)

Diethylether (700 mL), aniline (8.38 g, 90 mmol), and water (1.48 g, 82 mmol) were charged into a three-necked flask equipped with a dropping funnel and a condenser. A solution of vinyldimethylchlorosilane (11.6 mL, 82 mmol) in diethylether (50 mL) was added dropwise to the mixture (at 0 °C) with vigorous stirring. Stirring at this temperature was prolonged for further 15 min, and the precipitated solid (aniline hydrochloride) was then filtered off. After drying the resulting solution over $MgSO_4$, it was combined with triethylamine (7.51 g, 74 mmol) in a three-necked flask equipped with a dropping funnel and a condenser. A solution of dichloromethylsilane (3.5 mL, 34 mmol) in diethylether (50 mL) was added dropwise to the mixture (at 0 °C) with vigorous stirring. The precipitate (triethylamine hydrochloride) was filtered off and then the solvent was removed under reduced pressure to give a colorless liquid. Distillation of the residue under reduced pressure afforded the target monomer as a colorless liquid (3.77 g, 45%). IR (KBr, ν): 2961, 2152, 1408, 1257, 1059, 957, 910. ^{1}H NMR ($CDCl_3$, δ): 0.11 (d, 3H, J = 1.4 Hz, $SiCH_3$), 0.17 (s, 12H, $SiCH_3$), 4.65 (q, 1H, J = 1.4 Hz, SiH), 5.73 (q, 1H, J = 4.4 Hz, 19.4 Hz, SiCH=CH_2), 5.94 (q, 1H, J = 4.4 Hz, 14.9 Hz, SiCH=CH_2), 6.11 (q, 1H, J = 14.9 Hz, 19.4 Hz, SiCH=CH_2). ^{13}C NMR ($CDCl_3$, δ): 0.1, 1.5, 132.0, 138.9. ^{29}Si NMR ($CDCl_3$, δ): −35.4, −2.1.

2.1.2. Hyperbranched polysiloxysilane with vinyl end groups (HBPS-vinyl)

The AB_2-type monomer (18.49 g, 75 mmol) was charged into a two-necked flask and a Pt solution in xylene (0.75 mL, 0.075 mmol) was added (at 0 °C) with vigorous stirring. The system was then allowed to warm to room temperature and stirred for 15 h. The polymer was dissolved in diethylether (30 mL) and precipitated three times in methanol (300 mL). HBPS-vinyl was obtained as a colorless viscous liquid (8.31 g, 47%). M_n = 5400, M_w/M_n = 1.49. IR (KBr, ν): 2958, 2910, 2874, 1596, 1407, 1256, 1135, 1047, 955. ^{1}H NMR ($CDCl_3$, δ): −0.07 [br, SiCH(CH_3)Si], −0.01–0.18 (m, $SiCH_3$), 0.37, 0.43 (br, $SiCH_2CH_2Si$), 0.92–1.02 [m, SiCH_3(CH)Si], 5.71 (m, SiCH=CH_2), 5.91 (m, SiCH=CH_2), 6.13 (m, SiCH=CH2). ^{13}C NMR ($CDCl_3$, δ): −1.1, −0.2, 0.2, 0.6, 1.6, 8.1, 8.9, 9.6, 11.8, 131.7, 139.4. ^{29}Si NMR ($CDCl_3$, δ): −22.1, −21.8, −21.1, −20.5, −19.9, −4.8, −4.6, −4.5, −3.3, 7.0, 7.4, 7.6, 7.9, 8.1.

2.1.3. Hyperbranched polysiloxysilane with carboxyl end groups (HBPS-COOH)

Azobisisobutyronitrile (AIBN) (0.03 g, 0.2 mmol) was added to a mixture of HBPS-vinyl (1.00 g, 4.06 mmol), mercaptoacetic acid (0.41 g, 4.46 mmol), and toluene (15 mL) under argon flow. The mixture was stirred at 60 °C for 10 h and the solvent was evaporated. The residue was extracted with diethylether (150 mL) and washed three times with water (250 mL). A faint yellow viscous oil was

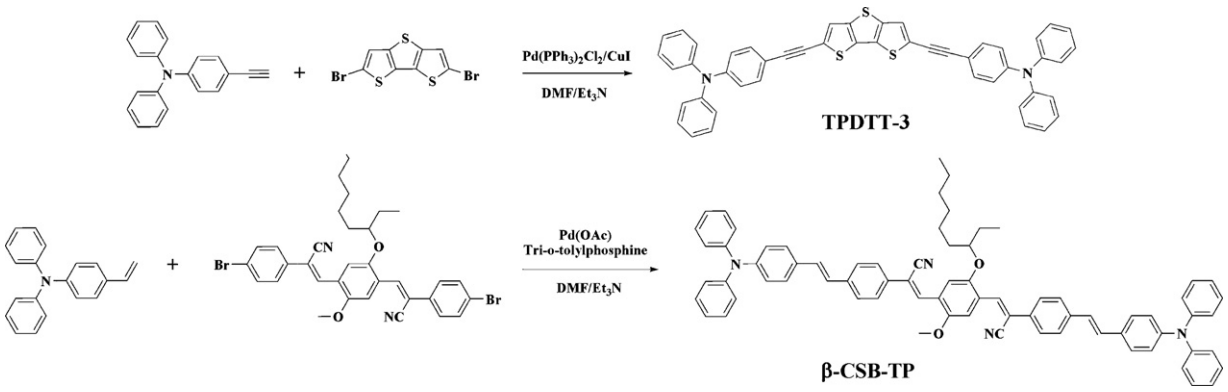

Scheme 2. Synthetic route for TPDTT-3 and β-CSB-TP.

obtained. Yield: 59% IR (KBr, ν): 3000, 2910, 1700. ^{1}H NMR (CDCl3, δ): −0.07 [br, SiC*H*(CH_3)Si], −0.01–0.18 (m, $SiCH_3$), 0.37, 0.43 (br, $SiCH_2CH_2Si$), 0.92–1.02 [m, SiCH_3 (CH)Si], 2.61 (m, CH_2CH_2S), 3.14 (s, SCH_2COOH), 11.2 (br, COOH). ^{13}C NMR ($CDCl_3$, δ): −1.3, −0.7, 0.1, 1.0, 7.6, 8.5, 9.0, 9.4, 11.5, 18.0, 27.4, 33.0, 177.0. ^{29}Si NMR ($CDCl_3$, δ): −21.9, −21.6, −20.9, −20.5, −19.9, 5.7, 7.9, 8.3. M_n = 5066, M_w = 8517, M_w/M_n = 1.68.

2.1.4. Hyperbranched polysiloxysilane with N,N-dimethylamino end groups (HBPS-N(CH_3)$_2$)

AIBN (0.03 g, 0.2 mmol) was added to a mixture of HBPS-vinyl (1.10 g, 4.50 mmol), 2-(dimethylamino)ethanethiol hydrochloride (1.90 g, 13.4 mmol), methanol (5 mL), and toluene (10 mL) under Ar atmosphere. The mixture was stirred at 60 °C for 15 h and the solvent was evaporated. The residue was extracted with diethylether (150 mL) and washed three times with 750 mL of NaOH (0.89 g, 22.3 mmol). The crude product was purified by separation GPC using tetrahydrofuran (THF) as eluent (Japan Analytical Industry Co., Ltd. LC-908, pump: HITACHI L-7110, column: JAIGEL-2H and JAIGEL-3H, RI detector: JAI RI DETECTOR RI-5). A faint yellow viscous oil was obtained. Yield: 78%. IR (KBr, ν): 2958, 2910, 2874, 2780. ^{1}H NMR ($CDCl_3$, δ): −0.06 [br, SiC*H*(CH_3)Si], −0.01–0.18 (m, $SiCH_3$), 0.30, 0.36 (br, $SiCH_2CH_2Si$), 0.8–1.02 (m, Si*CH*3 (CH)Si), 2.24 (s, NCH_3), 2.24, 2.59 (br, CH_2SCH_2), 4.20 (br, CH_2N). ^{13}C NMR ($CDCl_3$, δ): −1.3, −0.7, 0.1, 7.5, 8.6, 9.1, 11.5, 26.7, 29.3, 36.6, 45.1, 58.4. ^{29}Si NMR ($CDCl_3$, δ): −22.7, −22.5, −21.9, −21.4, −20.9, 4.9, 5.1, 7.4, 8.1, 10.8. M_n = 11,000, M_w = 19,000, M_w/M_n = 1.72.

2.1.5. The quaternary ammonium group in HBPS-N$^+$(CH_3)$_3$I$^-$

HBPS-N$^+$(CH_3)$_3$I$^-$ was synthesized according to procedures outlined in the literature (Ohara et al., 1983) using methyl iodide (0.062 mL), nitromethane (1 mL), and HBPS-N(CH_3)$_2$ (0.38 g) in DMSO (10 mL).

2.2. Synthesis of two-photon absorption chromophores

The dye 4,4′-[dithieno[3,2-*b*:2′,3′-*d*]thiophene-5,5′-diylbis(ethyne-2,1-diyl)bis(*N*,*N*-diphenylaniline)] (TPDTT-3) was prepared using the Sonogashira reaction, which involves a brominated dithienothiophene (Li et al., 2005) and a terminal alkyne bearing a triphenylamine (Suh et al., 1999). The chemical structure of TPDTT-3 is shown in Scheme 2. Briefly, 4-ethynyl-*N*,*N*-diphenylaniline (1.61 g, 6 mmol) was added dropwise into a solution of 2,6-dibromo-dithieno[3,2-*b*;2′,3′-*d*]thiophene (0.71 g, 2 mmol), bis(triphenylphosphine)palladium (II) chloride (3 mol.%), and copper(I) iodide (6 mol.%) in triethylamine (15 mL) at 60 °C. The mixture was refluxed for 24 h at 95 °C and cooled to rt. The reaction mixture is then poured into water and extracted with methylene chloride. The combined organic extracts were washed with water, dried over anhydrous $MgSO_4$, filtered, and the solvent was removed by evaporation. The product (bright green crystals, 1.02 g, yield: 70%) was purified using column chromatography (silica gel; hexane/methylene chloride 6:1). ^{1}H NMR (300 MHz, $CDCl_3$, δ) 6.99 (d, 4H, J = 8.4 Hz), 7.05–7.14 (m, 12H), 7.28–7.31 (m, 8H), 7.36 (d, 4H, J = 8.4 Hz), 7.49 (s, 2H). ^{13}C NMR (75 MHz, $CDCl_3$, δ) 148.75, 147.17, 141.71, 131.23, 132.60, 129.63, 125.35, 124.81, 124.75, 124.96, 122.14, 115.17, 95.67, 82.60. EIMS, *m*/*z*: 730 (100%, M$^+$). Anal. Calcd. for $C_{48}H_{30}N_2S_3$ (730.96): C, 77.38; H, 4.14; N, 3.83; S, 13.16. Found: C, 76.09; H, 4.24; N, 3.93; S, 13.14.

Synthetic route for the 1,4-bis(cyanostyryl)benzene (CSB) based chromophore is described in Scheme 2. The TPA molecule, β-CSB-TP, was synthesized by the Heck reactions of 4-(*N*,*N*-diphenylamino)styrene (Cho et al., 2004) with dibrominated bis(cyanostyryl)benzenes, 2,5-bis[2-(4′-bromophenyl)-2-cyanovinyl]-2-(2′-ethylhexyloxy)-5-methoxy-benzene (β-CSB-Br), (Tew et al., 2000) respectively. Briefly, β-CSB-Br (300 mg, 0.463 mmol), 4-(*N*,*N*-diphenylamino)styrene (310 mg, 1.108 mmol), $Pd(OAc)_2$ (5.1 mg, 0.014 mmol), tri-o-tolylphosphine (17.3 mg, 0.056 mmol) were dissolved in dry DMF (10 mL) and tributhylamine (2 mL), under nitrogen. The mixture was refluxed for 20 h at 140 °C and poured into methanol after cooling. The precipitate was collected by filteration. The product (298 mg, yield: 63%) was purified by column chromatography (silica gel; hexane/methylene chloride; 1/1 volume): ^{1}H NMR (300 MHz, $CDCl_3$, δ) 8.10 (s, 1H), 8.03 (s, 1H), 7.97 (s, 1H), 7.92 (s, 1H), 7.70 (t, 4H), 7.57 (d, 4H, J = 8.5 Hz), 7.41 (d, 4H, J = 8.5 Hz) 7.32–7.27 (m, 8H), 7.18–7.00 (m, 20H), 4.05 (d, 2H, J = 5.2 Hz), 3.99 (s, 3H), 1.89–1.78 (m, 1H), 1.55–1.32 (m, 8H), 1.00–0.91 (m, 6H). MS, *m*/*z*: 1028 (100%, M$^+$). Anal. Calcd. for $C_{73}H_{64}N_4O_2$ (1027.34): C, 85.18; H, 6.27; N, 5.44; O, 3.11. Found: C, 85.04; H, 6.17; N, 5.21.

2.3. Nanoparticle preparation

2.3.1. Preparation methodology of HBPS-C, HBPS-N, HBPS-CN nanoparticles

The HBPS-C nanoparticles were prepared by following a simple method: the HBPS-COOH was dissolved in DMSO (2 mM) and then 0.5 mL of polymer solution is diluted with 0.5 mL of DMSO. Water (9 mL) was added dropwise to a solution of HBPS-COOH in DMSO (1 mL, 1 mM) with vigorous stirring. The final concentration of dispersed nanoparticles in the mixed solution (water 90/DMSO 10, volume%) was 0.1 mM. After formation of the nanoparticles, excess DMSO was removed by dialysis of the solution against water in a 12–14 kDa cutoff cellulose membrane (Spectrum Laboratories, Houston) for 24 h. The dialyzed solution was then filtered through a 0.45 μm cutoff membrane filter (polytetrafluoroethylene, Whatman) and directly used for additional experimentation.

HBPS-$N^+(CH_3)_3I^-$ was used to prepare the HBPS-N nanoparticles, which were synthesized using the same procedure described for HBPS-C.

A mixed solution of HBPS-$N^+(CH_3)_3I^-$ and HBPS-COOH [HBPS-$N^+(CH_3)_3I^-$: 38 mg in 1 mL DMSO (2×10^{-3} M); HBPS-COOH: 19 mg in 1 mL of DMSO (2×10^{-3} M) was employed to prepare the HBPS-CN nanoparticles, which were synthesized in the same way as described for the HBPS-C nanoparticles, only changing the ratio of the HBPS-$N^+(CH_3)_3I^-$/HBPS-COOH solution using several polymer-weight percents [e.g., 90% HBPS-$N^+(CH_3)_3I^-$ + 10% HBPS-COOH to 10% C + 90% A, interval 10%].

2.3.2. Dye-loaded nanoparticles

Dye-loaded nanoparticles were prepared following the same procedure described for the HBPS-C nanoparticles, but now using either 0.5 mL TPDTT-3 or a β-CBS-TP solution (in DMSO, 0.5 mM) instead of 0.5 mL DMSO. The final concentration of dispersed nanoparticles in the mixed solution was 0.1 mM, including 25 μM TPDTT-3 or β-CBS-TP.

2.4. Material characterization

NMR spectra were recorded using a JEOL JNM-AL300 spectrometer with tetramethylsilane as the internal reference. Infrared spectra were recorded with a Jasco FT-IR-460 Plus spectrophotometer using a KBr pellet. UV–visible and photoluminescence spectra were measured using Shimadzu UV-3101 PC and Jobin-Yvon Fluorog FL-311 spectrofluorometers, respectively. The relative average molecular weights were determined by gel permeation chromatography (GPC) analysis using polystyrene standards for calibration (Japan Analytical Industry Co., Ltd. LC-908, pump: HITACHI L-7110, column: JAIGEL-2H and JAIGEL-3H, RI detector: JAI RI DETECTOR RI-5). The effective size, size distribution, and ζ potential of the nanoparticles were determined by utilizing a dynamic light-scattering particle-size analyzer (Brookhaven Zeta-Plus fitted with an avalanche photodiode detector using a 656-nm laser, Brookhaven Instruments Corporation of Holtsville, NY). A dialyzed solution containing all the nanoparticles was passed through a 0.45 μm-cutoff membrane filter (polytetrafluoroethylene) and directly used for analyzing. Transmission electron microscopy (TEM) was performed using a JEOL JEM-100cx microscope at an accelerating voltage of 80 kV.

2.5. Two-photon absorption cross-section measurements

TPA cross-sections were measured using a two-photon-induced fluorescence method (Xu and Webb, 1996; Albota et al., 1998) in DMSO solutions and water dispersions. Samples such as TPDTT-3 and the reference were measured using a concentration of 2.5 μM. The laser system was composed of a mode-locked Ti–sapphire laser (Mira from Coherent), with 130-femtosecond (fs) pulses at a repetition rate of 76 MHz, pumped by a diode-pumped solid-state (DPSS) laser (Verdi from Coherent) which was used for excitation. A spectrum analyzer (IST-rees) was employed to monitor the excitation wavelengths. The laser beam was focused onto the sample using a 5 cm-focal-length lens and the fluorescence spectra were monitored using a Jobin-Yvon Fluorolog-3 spectrometer.

2.6. Cell viability

Cos-7 adherent kidney cell lines derived from African green monkey kidney cells were dispensed into a 96-well flat-bottomed microplate (Nunc) at a concentration of 10,000 cells/well and allowed to attach overnight (using minimum essential medium alpha, MEMα, and 10% FBS for growth). Cell viability was assessed using the Cell Titer-Glo™ luminescent cell viability assay (Promega Corporation, Madison, WI). This assay is a homogenous method for determining the number of viable cells in culture based on the quantity of ATP present, which signals the existence of metabolically active cells. In brief, a Cell Titer reagent was added to the cells after the experiments and the samples were mixed for 2 min and allowed to incubate for 10 min at room temperature. Luminescence was measured using a microplate luminometer (Synergy HT microplate reader Bio-Tek), and the data were expressed as a percentage of the control. The tests were performed at least four times. Each point represents the mean ± SD value (bars) of replicates of one representative experiment.

2.7. In vitro studies with tumor cells (nanoparticle uptake, two-photon-excited fluorescence imaging, flow cytometry)

Human cervical epithelioid carcinoma cell lines (HeLa) and African green monkey kidney (Cos-7) cells were cultured according to the American Type Culture Collection (ATCC, Manassas, VA). To study the uptake and imaging properties of the HBPS nanoparticles, the cells were first plated (at approximately 300,000 cells per culture plate, using 35 mm glass-bottom plates from MatTek Corporation) and then the corresponding full medium was added (2 mL). For the flow cytometry studies, the cells were plated in 25 cm^2 culture flasks (at approximately 700,000 cells per flask) and 4 mL of corresponding media was added. The plates and flasks were then placed in an incubator at 37 °C with 5% CO2 (VWR Scientific, model 2400). After 24 h of incubation, the cells (about 60% confluency) were rinsed with phosphate buffered saline (PBS), and a fresh medium was added. For the imaging experiments, the respective nanoparticle samples (100 μL) were added to the cell-culture medium (1 mL) and the medium in each plate was exchanged with the nanoparticle-mixed medium. For the flow cytometry measurements, the nanoparticle suspensions (200 μL) were mixed with the cell-culture medium (2 mL), and the medium in each flask was exchanged with this nanoparticle-containing medium. Culture plates and flasks were returned to the incubator. After incubation in the presence of the nanoparticles (between 30 min and 3 h), the culture plates and flasks were washed thoroughly with PBS to remove any free nanoparticles. A fresh medium without serum was added to the 35 mm culture plates for confocal/two-photon imaging; this medium was directly imaged under a confocal microscope (Leica TCS SP2-AOBS). Confocal images were acquired using 405 nm diode-laser excitation, whereas the two-photon images were acquired using 800 nm excitation (140 fs pulses at 76 MHz repetition rate) from a Ti:sapphire laser (Mira from Coherent Inc.) pumped by a 10 W DPSS laser (Verdi from Coherent Inc.). For the flow cytometry measurements, the medium was removed and the cells were detached using ethylenediaminetetraacetic acid (EDTA) and trypsin. Cell pellets were collected by centrifugation (2000 rpm, 5 min) and resuspended in PBS. Cell suspensions were analyzed using a FACSCalibur flow cytometer (equipped with the 488 nm line from an argon-ion laser). We used absorption and fluorescence spectroscopy to confirm that there is sufficient fluorescence signal from β-CSB-TP under the 488 nm excitation. Data analyses were conducted using the WinMDI program (version 2.8).

2.8. Agarose gel electrophoresis

Aqueous dispersions of HBPS-C, HBPS-N, HBPS-CN30:70, and HBPS-CN10:90 were gently mixed with DNA (phospho-β-galactosidase: p-β-gal) (0.4 μg) in diethylpyrocarbonate (DEPC) treated water at room temperature and incubated overnight (at 4 °C) for the formation of the DNA–nanoparticle complex. The above solution, or 0.4 μg of free DNA as control, was added to 1% agarose gel in a Tris acetate–EDTA (TAE) buffer and subsequently stained with ethidium bromide. The gel was run for 1 h (at 90 V) and doc-

umented using a UVP bioimaging system. An LM-20E ultraviolet benchtop transilluminator (UVP, Upland, CA) was used in conjunction with an Olympus (Melville, NY) Digital Camedia C-4000 zoom color camera with a UV filter and a lens. Documentation was completed using the DOC-IT system software.

2.9. In vitro gene transfection using β-galactosidase plasmid

Cos-7 cells were seeded in a 24-well plate (at a density of 40,000 cells per well) in 1 mL of minimum essential medium alpha (MEMα, Invitrogen, CA) containing 10% fetal bovine serum (FBS). After 24 h of incubation, the cells were washed and maintained for 1 h in the medium without serum. The DNA-complexed suspensions were prepared using 1 μg of plasmid and different amounts of HBPS nanoparticles (namely, 5, 10, 15, and 20 μL) and incubated for 6 h (at room temperature) to form the DNA–nanoparticle complex. The DNA-complexed HBPS nanoparticle suspensions (200 μL) were then added into the wells. Transfection experiments were performed in a medium without serum protein. After 4 h of incubation, the medium was replaced with fresh MEMα containing 10% FBS and incubated (at 37 °C) with 5% CO_2 (VWR Scientific, model 2400). The cells were left for 36 h in the incubator, washed once with PBS, and analyzed for β-gal expression using a mammalian β-galactosidase assay kit (Pierce Biotechnology, IL). The absorbance was measured at 405 nm using a microplate reader (Synergy HT, Bio-Tek). Transfection measurements with Fu-Gene6 (Roche Applied Systems, IL) pSV-β-gal plasmid were performed (as positive controls) according to the manufacture's protocol. Briefly, the Fu-Gene6-DNA (2 μL/1 μg) complexes were incubated in 200 μL of fresh medium without serum protein for 30 min, the cells being incubated further (for 36 h) at 37 °C before being analyzed for β-gal activity. Cells treated with either media alone or media containing 1 μg of DNA were used as control. The data are expressed as the mean of triplicate samples after subtraction of the DNA only group, plus/minus the standard deviation of the mean.

2.10. In vitro gene transfection using pEGFP-N1 plasmid

Cos-7 (or MCF-7) cell lines were cultured as previously described. Highly purified pEGFP-N1 was transfected in the Cos-7 (or MCF-7) cells using the Fu-Gene6 transfection reagent and according to the manufacturer's protocol. Fu-Gene6 served as control to deliver 1 μg of pEGFP-N1 into the cells. Nanoparticle suspensions prepared by adding 1 μg of pEGFP-N1 plasmid and 20 μL of HBPS nanoparticles (HBPS-C, HBPS-N, HBPS-CN30:70, and HBPS-CN10:90) in media without serum (200 μL) were incubated for 6 h at room temperature before the experiments and added to the 35 mm culture plates. After 4 h of incubation, the medium was replaced by fresh MEMα containing 10% FBS, and incubated at 37 °C with 5% CO_2 (VWR Scientific, model 2400). Fluorescence images were acquired after 36 h under a fluorescence microscope (MRC-1024, Bio-Rad, Richmond, CA), which was attached to an upright microscope (Nicon model Eclipse E800). A water-immersion objective lens (Nikon, Fluor 60×, NA1.0) was used for the cells.

2.11. Amplification and purification of pEGFP-N1

EGFP-N1 (Clontech) pDNA grown in *Escherichia coli* DH5α was purified using the Qiagen kit according to the manufacturer's instructions and resuspended in TE buffer (10 mmol/L Tris/HCl and 1 mmol/L EDTA, pH 8.0). The purity was confirmed using 1% agarose gel electrophoresis and spectrophotometry (A260/A280), and the DNA concentration was measured by UV absorption spectroscopy performed at 260 nm (ND-1000 Spectrophotometer).

3. Results and discussion

3.1. Material preparation and characterization

The synthetic routes for obtaining the silicone-based polymers are described in Scheme 1. HBPS containing vinyl end groups (HBPS-vinyl) was synthesized by hydrosilylation of 1,1,3,5,5-pentamethyl-1,5-divinyltrisiloxane (an AB_2 type monomer), whereas HBPS polymers containing carboxyl (HBPS-COOH) and *N*,*N*-dimethylamino [HBPS-N$(CH_3)_2$] end groups were prepared by the reaction of HBPS-vinyl with mercaptoacetic acid and 2-(dimethylamino)ethanethiol hydrochloride, respectively. The compound HBPS-N$(CH_3)_3{}^+I^-$ was prepared by quaternization of the amine group on HBPS-N$(CH_3)_2$. The chemical structures and average molecular weights were fully characterized using ^{1}H NMR, ^{29}Si NMR, FTIR, and GPC. The carboxyl end groups of the side chains bind to the polysiloxysilane backbone, thus allowing micelle formation in aqueous media. In a similar manner, quaternary ammonium components attach to the side chains, thereby producing a material that contains cationic ammonium salt groups to promote hydrophilicity. The presence of carboxyl and quaternary ammonium substituents in the side chains enables the formation of amphiphilic polysiloxysilane nanoparticles by means of self-assembly in aqueous media.

The ability of each polymer to form nanoparticles in aqueous dispersions was examined by using dynamic light scattering (DLS) and TEM. Fig. 1a shows representative nanoparticle size distributions for HBPS-C and HBPS-N, while Fig. 1b displays the corresponding TEM images. The size distributions and ζ potentials (index of surface charge) of the nanoparticles were monitored by DLS (Brookhaven 90Plus with ZetaPlus attachment). The DLS and ζ potential data are shown in Table 1. For each type of nanoparticle, a stable aqueous dispersion was obtained by slowly adding a given amount of polymer solution in *N*,*N*-dimethyl sulfoxide (DMSO) to water to obtain a final concentration of 10 μM. Although the prepared nanoparticles exhibited a narrow size distribution, they had different surface charges depending on the mixture of HBPS polymers used. The size of the polysiloxysilane nanoparticles depends on both the polymer concentration and the stirring speed. Particle sizes below 60 nm were obtained using a stirring speed of 1200 rpm and a polymer concentration of 10 μM. The HBPS-N nanoparticles generated from HBPS-N$^+(CH_3)_3I^-$ showed a positive surface charge density (ζ potential) which might be desirable for binding to negatively charged DNA molecules. A positive ζ potential may also be beneficial for enhanced cellular uptake because typical cell membranes are slightly negatively charged. On the other hand, the HBPS-C nanoparticles generated from HBPS-COOH exhibit a negative ζ potential.

The nanoparticle surface can be modified to have different ζ potentials by using an appropriate mixture of HBPS molecules containing different charged groups attached to it. This altered charge distribution of the nanoparticles is beneficial for drug/fluorescent-probe carrier systems, because the charge tunable nanoparticles might provide the effective accumulation in the target cells. Thus, we have developed surface-charge-controllable nanoparticles with various altered surface charges. The HBPS-CN30:70 nanoparticles (prepared form a mixture of 70 mol.% HBPS-N$^+(CH_3)_3I^-$ and 30 mol.% HBPS-COOH) are stable in aqueous dispersions and exhibit a suitable size (see Fig. 1). Also, their surface charges have a ζ potential that seems to be in-between the ζ potential of nanoparticles prepared from positively charged HBPS-N$^+(CH_3)_3I^-$ and that of nanoparticles obtained from negatively charged HBPS-COOH. Therefore, variable values of the ζ potential can be obtained by simply mixing HBPS-N$^+(CH_3)_3I^-$ and HBPS-COOH (see Fig. 2). Several ratios of the constituents of the HBPS blends were explored systematically for preparing the surface-charge-controllable nanoparticles. Table 1 shows the mixing ratios and

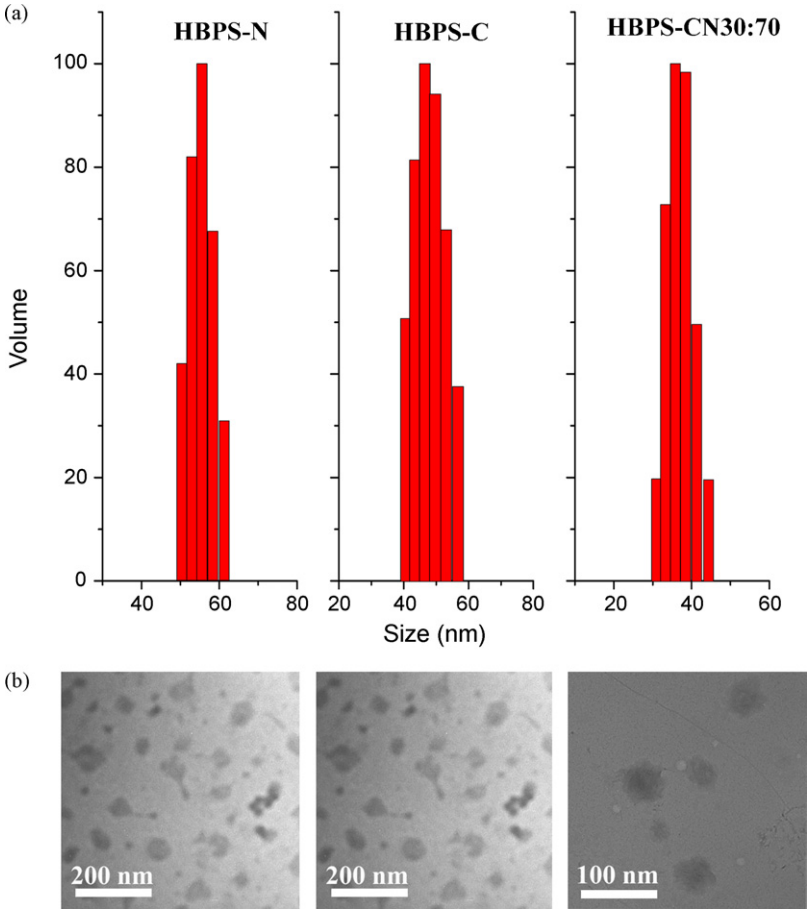

Fig. 1. (a) Representative DLS data showing the nanoparticle size distributions of polysiloxysilane nanoparticles, HBPS-N (nanoparticles prepared by HBPS-$N^+(CH_3)_3I^-$), HBPS-C (nanoparticles prepared by HBPS-COOH), and HBPS-CN30:70 (particles formed by mixing ratio of 30 mol.% of HBPS-COOH and 70 mol.% of HBPS-$N^+(CH_3)_3I^-$). (b) TEM images of the corresponding samples.

characteristics of the nanoparticles. At ratios between 5:5 and 3:7 [HBPS-$N^+(CH_3)_3I^-$:HBPS-COOH, in mol.%], the particles settled down during dialysis. Typically, the surface charges on the nanoparticles play a significant role in their stabilization in an aqueous environment. If the particles prepared from mixed polymers have a minimal surface charge density (i.e., close to neutral), their stability in aqueous dispersions may be affected. Still, stable nanoparticle dispersions with a wide range of ζ potentials can be obtained by simply adjusting the ratio of the two HBPS polymers. Here, we mainly study in detail one mixing ratio, namely, HBPS-CN30:70 (70 mol.% HBPS-$N^+(CH_3)_3I^-$ and 30 mol.% HBPS-COOH) because of the stability, size, and uptake efficiency.

The HBPS nanoparticle systems were found to be very efficiently loaded with hydrophobic molecules in aqueous media. The hydrophobic molecules such as fluorescent dyes and drugs are encapsulated inside the HBPS nanoparticles, thereby forming hydrophobic interaction-induced micelles. To demonstrate this capability of encapsulation, we chose a two-photon-absorption (TPA) dye, namely, 4,4′-[dithieno[3,2-*b*:2′,3′-*d*]thiophene-5,5′-diylbis(ethyne-2,1-diyl)bis(*N*,*N*-diphenylaniline)], to be encapsulated inside the HBPS nanoparticles. We selected this dye because it exhibits the following characteristics: the new dithieno[3,2-*b*:2′,3′-*d*]thiophene (DDT) based dye possesses a large value of the TPA cross-section (σ_2), a high fluorescence quantum yield, good solubility in common solvents, and a high thermal/optical stability. Thus, HBPS nanoparticles containing TPDTT-3 dyes can be used as efficient two-photon fluorescence labels for bioimaging. Chemical structures of the DTT-based TPA chromophores are described in Scheme 2. The dye TPDTT-3 shows a solvatochromic behavior that depends on the polarity of the solvent; for example, fluorescence from a highly polar *N*,*N*-dimethylformamide (DMF) solution is red-shifted and slightly quenched compared to a nonpolar toluene solution of the same dye (Fig. 3). The changes in the emission wavelength should be monitored during TPA-dye encapsulation inside

Table 1
Characteristics of the hyperbranched polysiloxysilane nanoparticles.

Type of nanoparticle	Polymer	Zeta potential (mV)[a]	Mean size (nm)	
			TEM	DLS[a]
HBPS-N	HBPS-$N^+(CH_3)_3I^-$	64 ± 8	~40	55 ± 6
HBPS-C	HBPS-COOH	−40 ± 9	~32	46 ± 10
HBPS-CN30:70[b]	HBPS-COOH and HBPS-$N^+(CH_3)_3I^-$	46 ± 6	~40	38 ± 8

[a] The data represent the mean ± SD (standard deviation), $n = 3$.
[b] A mixture of 30 mol.% HBPS-COOH and 70 mol.% HBPS-$N^+(CH_3)_3I^-$. Particle sizes below 60 nm were obtained using a stirring speed of 1200 rpm and a polymer concentration of 10 μM.

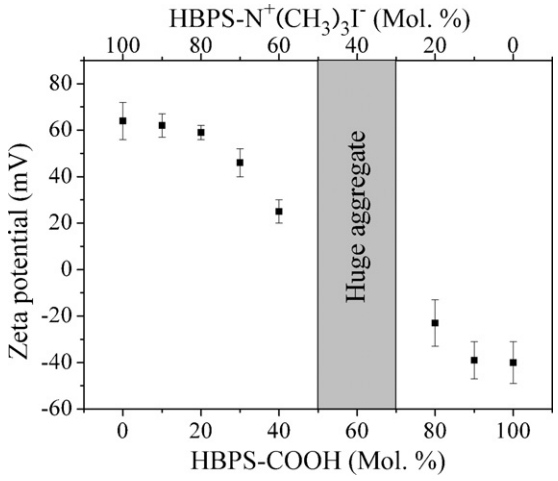

Fig. 2. Zeta-potential changes of HBPS-CN according to the mixed ratio.

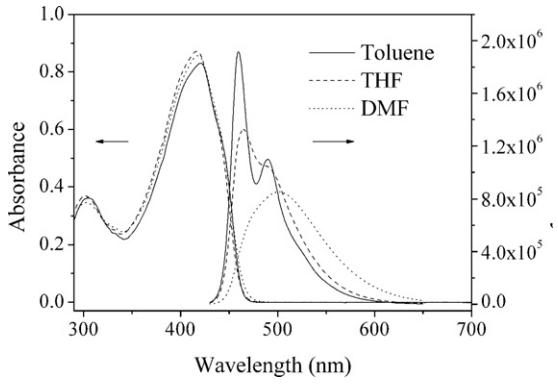

Fig. 3. One-photon absorption and emission spectra of TPDTT-3 in various solvents.

Table 2
One- and two-photon photophysical properties of DTT-based chromophores and polysiloxysilane nanoparticles.

Compound	Solvent	λ_{max}^{abs} (nm)[a]	λ_{max}^{flu} (nm)[b]	ϕ_f[c]	σ_2 (GM)[d]	λ_{max}^{TPE} (nm)[e]
TPDTT-3	DMSO	420	516	0.45	1509	760
HBPS-C	Water	405	462	0.15	344	760
HBPS-N	Water	405	462	0.09	260	760

[a] One-photon absorption maximum.
[b] One-photon fluorescence maximum.
[c] Fluorescence quantum yield determined relative to rhodamine 6G.
[d] TPA cross-section; 1 GM = 10^{-50} cm^4 s photon^{-1}, measured by the two-photon fluorescence method using 130 fs pulses at a repetition rate of 76 MHz.
[e] TPA maximum wavelength.

the HBPS nanoparticles. Such changes can be utilized to confirm encapsulation of the dye inside the hydrophobic environment of the HBPS nanoparticles.

For each type of dye-loaded nanoparticle, we obtained stable aqueous dispersions in the same manner as described above. The final concentration of the polymer in water was 0.1 mM, including 25 μM TPDTT-3. The TPDTT-3 loaded HBPS-C nanoparticles (i.e., the nanoparticles prepared using HBPS-COOH) show specific changes in the fluorescence spectra depending on the molecular environments. Fig. 4a clearly shows the drastic changes in the emission spectrum of TPDTT-3 loaded HBPS-C in comparison with those of the dye dispersed in water or dissolved in DMSO. The structured bands observed in the emission spectrum of HBPS-C are blue-shifted relative to the featureless broadband emissions observed in the spectra of the same dye in DMSO or water. In addition, TPDTT-3 loaded HBPS-C exhibits the same emission behavior as TPDTT-3 in an HBPS-COOH spun film. Therefore, encapsulation of TPDTT-3 by HBPS-COOH leads to important photophysical changes in this system. In contrast, the nanoparticles that do not contain the TPA dye show no absorption in the wavelength range of 300–800 nm (see Fig. 4c). These changes indicate that the dye must be encapsulated inside the polymer nanoparticles during their formation, by means

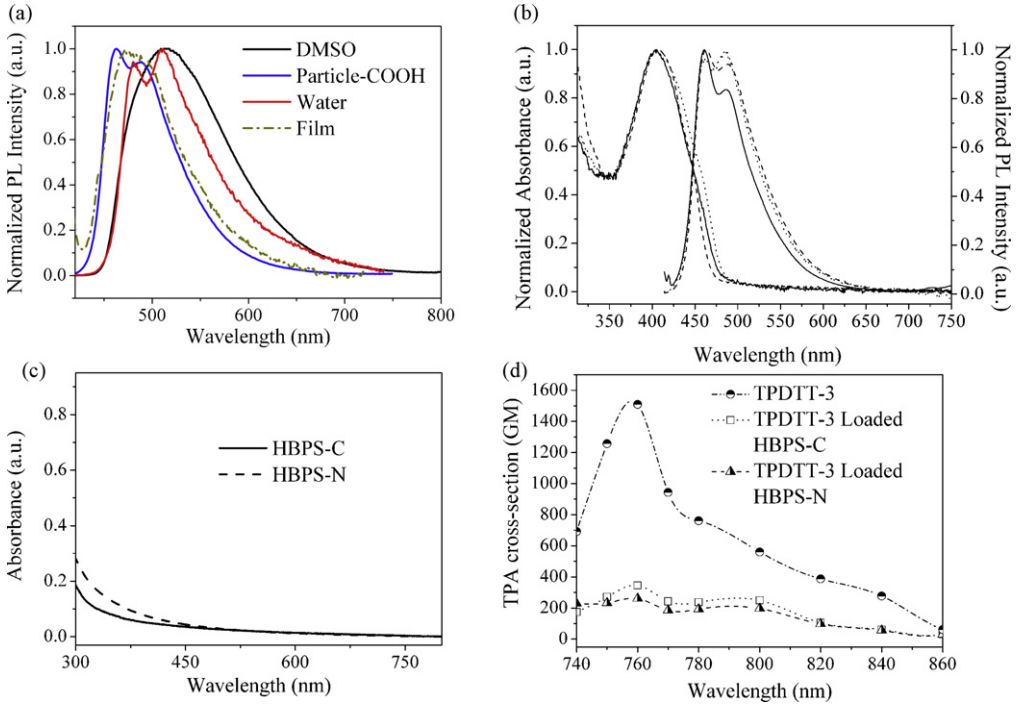

Fig. 4. (a) Emission changes of TPDTT-3 according to the molecular environments. (b) One-photon absorption and emission spectra of three type TPDTT-3 loaded polysiloxysilane nanoparticles (solid line: HBPS-C, dash: HBPS-N, dash-dot: HBPS-CN30:70). (c) One-photon absorption spectra of only HBPS nanoparticles. (d) Two-photon excitation spectra of free TPDTT-3 and TPDTT-3 loaded nanoparticles. 1 GM = 10^{-50} cm^4 s photon^{-1}.

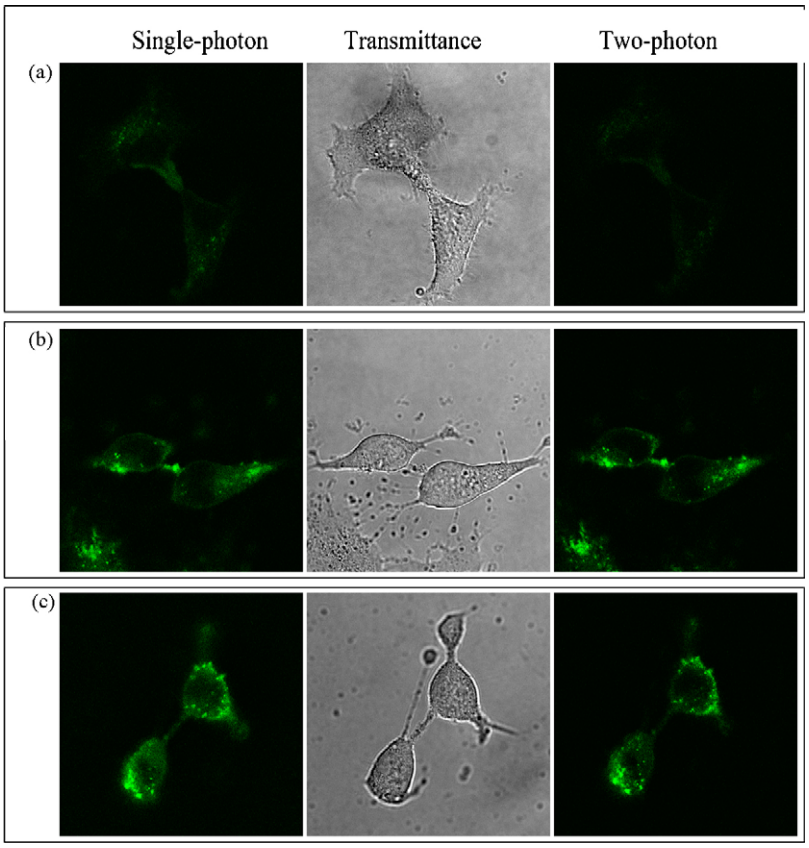

Fig. 5. Confocal fluorescence microscopy images of HeLa cells treated with TPDTT-3 loaded HBPS-C (a), HBPS-CN30:70 (b), and HBPS-N (c) for 3 h. The single photon excitation (left column), transmittance (middle) and two-photon excitation (right) images are shown.

of hydrophobic interactions between the TPA dye and the polymer backbone. Representative spectra of the three types of nanoparticles after loading with TPDTT-3 are shown in Fig. 4b. The similarities between the one-photon-absorption and the fluorescence spectra suggest that both absorption and emission occur from the same environments.

The TPA properties of TPDTT-3 loaded polysiloxysilane nanoparticles were studied by two-photon-excited fluorescence (TPEF) measurements using a Ti–sapphire laser with 130 fs pulses at a repetition rate of 76 MHz (Mira from Coherent Inc.). Fig. 4d shows the two-photon excitation spectrum, recorded in the range of 720–860 nm and plotted together with that of the reference, rhodamine 6G (Krebs and Spanggaard, 2002; Strehmel et al., 2003). The TPA spectra of both types of nanoparticles showed hypsochromic shifts in intensity relative to the TPDTT-3 DMSO solution (1509 GM). This intensity decrease indicates that TPDTT-3 may be locally aggregated inside the nanoparticles and that the environment changes

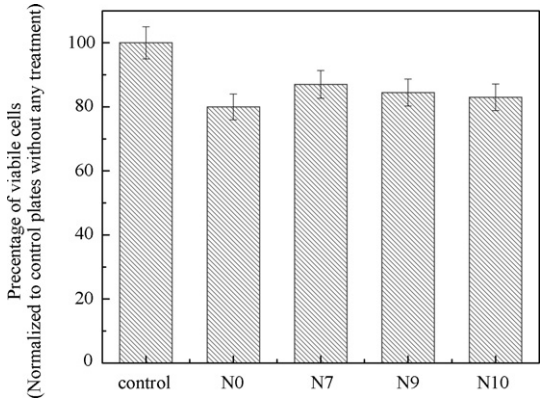

Fig. 6. Percentage of Cos-7 cell survival after treatment (for 24 h) with the HBPS nanoparticles (10 μL).

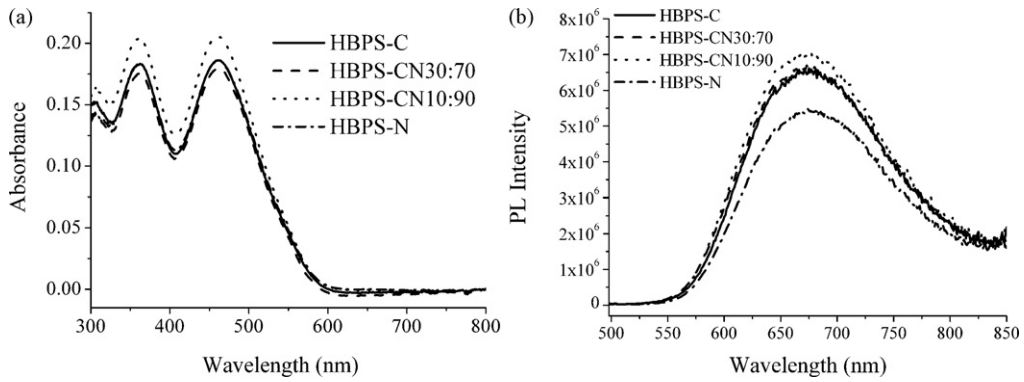

Fig. 7. Absorption (a) and emission (b) spectra of β-CBS-TP loaded HBPS nanoparticles. The emission spectra were recorded using an excitation wavelength of 488 nm.

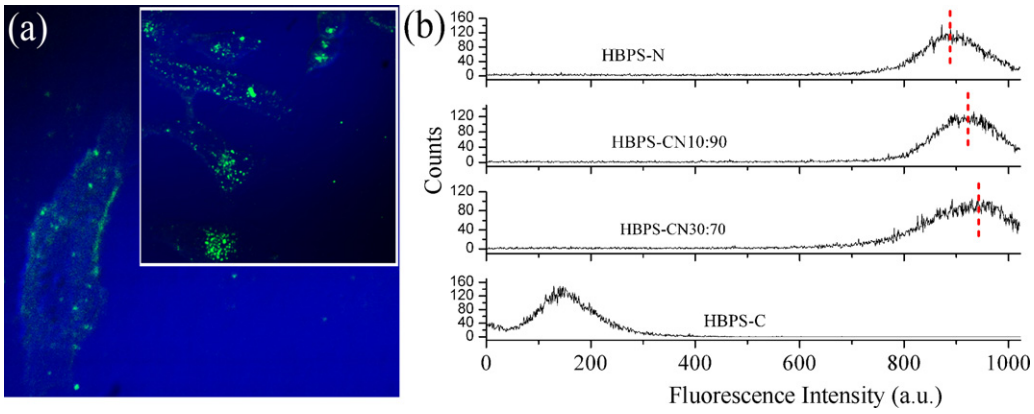

Fig. 8. One photon excitation images of HeLa cells treated with TPDTT-3 loaded HBPS-N for 30 min. Inset; 3 h staining. Note that merged transmission (blue) and single-photon excited fluorescence (green) images are shown. (b) Flow cytometry histograms of the nanoparticles in HeLa cells. In all cases, 20,000 cells were counted and all data were gated in a similar way. (For interpretation of the references to color in this figure legend, the reader is referred to the web version of the article.)

around the TPA dyes by encapsulation of the polymer. The estimated σ_2 values at 760 nm are 344 GM for HBPS-C and 260 GM for HBPS-N. All the collected TPA data are shown in Table 2.

3.2. *In vitro one- and two-photon bioimaging*

Structurally similar polysiloxysilane nanoparticles, with different surface charges and loaded with the TPA dye, were evaluated as optical bioimaging probes using multi-photon and confocal microscopy. Studies were conducted to evaluate the cellular-uptake capabilities of the HBPS nanoparticles into human cervix epithelioid carcinoma (HeLa) cells. Cells in culture media, containing TPDTT-3 loaded HBPS-C, HBPS-N, and HBPS-CN30:70, were independently incubated for 3 h. Fig. 5 shows the single-photon confocal and two-photon images of HeLa cells treated with the composite nanoparticles. As the imaging results show, the composite nanoparticles were similarly internalized into the cell cytoplasm, with minimal cytotoxic effect. Although all the composite nanoparticles showed a comparable intracellular distribution, their cellular uptake significantly depended on their surface-charge density. We also confirmed minimal cytotoxicity of the nanoparticles using the CellTiter-Glo™ luminescent cell viability assay, based on measurements of the cellular ATP levels, which showed a minimal decrease in the number of viable cells, even after 12 h of incubation (Fig. 6).

Even though two-photon fluorescence imaging gives cellular-uptake-efficiency information for a limited number of cells, it does not provide enough statistical information on the difference in cellular uptake of the composite nanoparticles depending on their surface charges. Therefore, flow cytometry was employed to understand the effect of nanoparticle surface charge on both cellular uptake and signal output from cells, using TPA-loaded HBPS-C, HBPS-N, HBPS-CN30:70, and HBPS-CN10:90 under excitation at 488 nm. It should be noted that we had to prepare β-CBS-TP (see Scheme 2) loaded HBPS nanoparticles for the flow cytometry studies, because the excitation wavelength of 488 nm was not optimal for the TPDTT-3 dye. The β-CBS-TP loaded HBPS nanoparticles produced a fluorescence signal that was good enough to be detected using flow cytometry (see Fig. 7). Note that the signal output from the stained cells is proportional to both the fluorescence intensity and the cellular-uptake efficiency of the individual nanoparticles.

As seen from the flow-cytometry results in Fig. 8b, the highly negative surface charges of the HBPS-C nanoparticles (from the carboxylic acid end groups in the HBPS-COOH polymer) had a negative effect on cellular uptake, relative to nanoparticles with positive surface charges (e.g., HBPS-CN30:70). This can be explained because it is well known that a highly negative ζ potential gives rise to electrostatic repulsion that reduces the cellular uptake of nanoparticles (because the surface of a cell membrane is negatively charged). In contrast, the positive ζ potential of the HBPS-N nanoparticles can be regarded as a key factor by which the nanoparticles are attracted to the slightly negatively charged cell membrane. As seen from Fig. 8, while after 30 min incubation (Fig. 8a) of HBPS-N, most of the fluorescent nanoparticles accumulated in the cell membranes. After 3 h of incubation (Fig. 8a inset) fluorescence image showed significantly entry of HBPS-N into the cell cytoplasm. These results

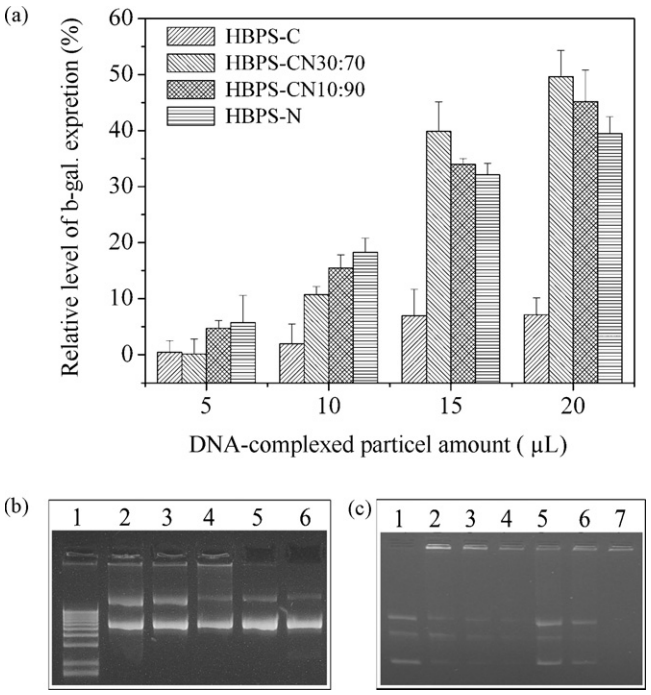

Fig. 9. (a) Relative transfection efficiency of β-galactosidase expression in COS-7 cells using HBPS nanoparticles. The graph for each transfection represents the mean of two separate experiments in which each sample was tested in triplicate. For comparison purposes, in each nanoparticle types, the levels of β-gal expression were adjusted to show relative expression by normalizing the β-gal expression of the Fu-Gene6 vector to 100%. Each point represents the mean ± SD (bars) of replicates. (b) Image of agarose gel electrophoresis of plasmid DNA, free and complexed with HBPS nanoparticles. Lane 1: molecular weight marker, lane 2: HBPS-N/DNA, lane 3: HBPS-CN10:90/DNA, lane 4: HBPS-CN30:70/DNA, lane 5: HBPS-C/DNA, lane 6: free DNA. (c) Displays binding efficiency of DNA with HBPS at different DNA ratios (studied by agarose gel electrophoresis). Lane 1: DNA (40 ng/μl), lane 2: HBPS-CN10:90 (200 μL)/DNA (4 μL), lane 3: HBPS-CN10:90 (400 μL)/DNA (4 μL), lane 4: HBPS-CN10:90 (800 μL)/DNA (4 μL), lane 5: HBPS-CN30:70 (200 μL)/DNA (4 μL), lane 6: HBPS-CN30:70 (400 μL)/DNA (4 μL), lane 7: HBPS-CN30:70 (800 μL)/DNA (4 μL).

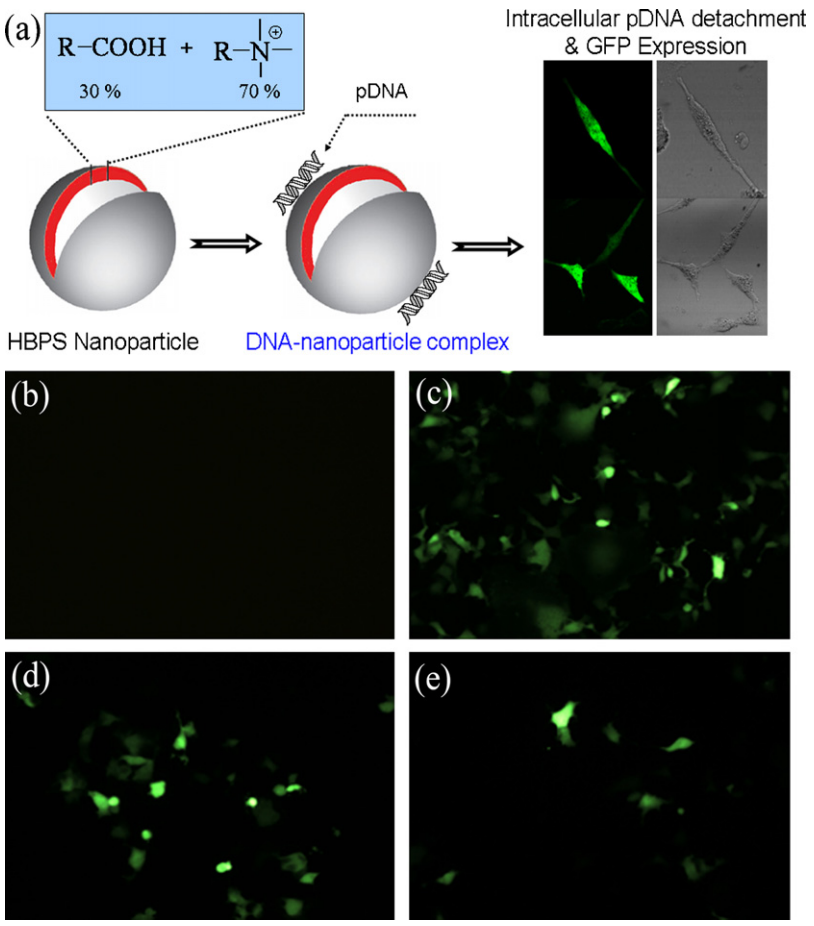

Fig. 10. The schematic diagram for gene delivery using HBPS nanoparticles (a). Confocal fluorescence image of Cos-7 cells treated with HBPS nanoparticles previously incubate with EGFP plasmid. Transfected images of Cos-7 cells with EGFP-encoding plasmid with different carriers (b) naked pDNA, (c) Fu-Gene6 transfection reagent, (d) complex HBPS-CN30:70/EGFP plasmid, and (e) complex HBPS-N/EGFP plasmid.

indicate that the cationic variant of the HBPS nanoparticles (i.e., HBPS-CN30:70) exhibit better cellular-uptake efficiency.

3.3. *In vitro gene delivery*

As mentioned previously, surface-charge-tunable HBPS-based nanoparticles possess a number of advantages that can be used in the delivery of genetic molecules (e.g., plasmid DNA: pDNA). These advantages include a strong attraction to the genetic molecules via coulombic interactions in aqueous media as well as the effectively release of genetic molecules inside targeted cells by buffering effect (Xu and Szoka, 1996) or proton sponge effect (Boussif et al., 1995). These properties of the nanoparticles make them highly appropriate for use as nonviral gene delivery vectors. We performed agarose gel electrophoresis studies to examine the binding efficiencies of DNA molecules to these cationic HBPS nanoparticles (e.g., HBPS-CN30:70). The results obtained for pDNA-both free and complexed with different HBPS nanoparticles (namely, HBPS-C, HBPS-N, HBPS-CN30:70 and HBPS-CN10:90) are shown in Fig. 9b. It can be seen that with increasing amounts of quaternary ammonium groups (positive charge) on the nanoparticles, the mobility of the complexed DNA toward the positive terminal is retarded (see Fig. 9c). This result suggests that the plasmid is no longer able to move freely, because the resulting nanoparticle–DNA complex has a restricted mobility in the gel. These observations indicate an excellent complexing ability of the cationic HBPS nanoparticles with pDNA, which is an important pre-requisite for its use as gene delivery vector.

The second requirement for use in gene delivery is an efficient release of the functional genetic material inside the cell cytoplasm, after facilitating the uptake of plasmid DNA into the cells. To confirm that the delivered DNA is functional, we studied the delivery of two different plasmid vectors encoding enhanced green fluorescence protein (eGFP) and β-galactosidase (β-gal) using HBPS nanoparticles. The transfection efficiencies of the encoded proteins after delivery were monitored using either confocal microscopy (for eGFP) or spectrophotometric methods (for β-gal).

As shown in Fig. 10, we observed that the cells were transfected with plasmid encoding EGFP (pEGFP) for HBPS-N, HBPS-CN30:70, and HBPS-CN10:90 nanoparticles as the delivery vector. The observed green cellular fluorescence is from the expressed EGFP, which has been confirmed by confocal fluorescence microscopy. It is very well known that cationic materials can mediate gene delivery. Thus, in addition to the transfection of Cos-7, we report preliminary experiments to examine the transfection ability of the HBPS-based vectors to other cell type such as MCF-7 (human breast tumor cells). The resulting fluorescence microscopy images of the EGFP transfected MCF-7 are shown in Fig. 11. For a given gene delivery system, the HBPS-CN30:70 shows better transfection efficiency compared with HBPS-CN10:90 and HBPS-N. Behr and his coworkers have investigated that the proton sponge effect is responsible for the release of DNA into the cytoplasm by cationic polymers with pK_as below physiological pH (Boussif et al., 1995). A moderate positive charged HBPS nanoparticles, HBPS-CN30:70, are notable as a proton sponge, leading to high transfection activity against highly positive charged nanoparticle (HBPS-N).

Spectrophotometric methods were applied to monitor the dependence of the *in vitro* gene transfection efficiency on the

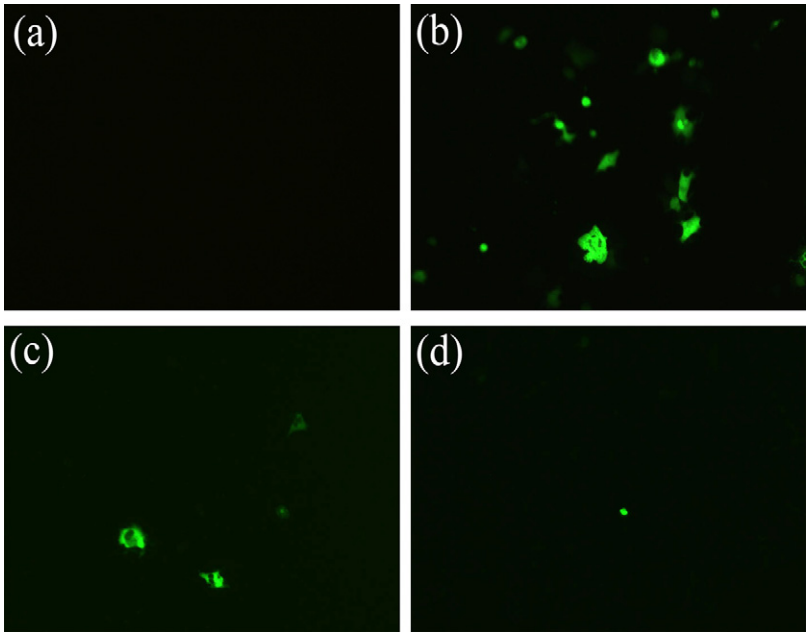

Fig. 11. Confocal fluorescence image of MCF-7 cells treated with HBPS nanoparticles previously incubated with EGFP plasmid. Transfected images of MCF-7 cells with EGFP-encoding plasmid with different carriers (a) naked pDNA, (b) complex HBPS-CN30:70/EGFP plasmid, (c) complex HBPS-CN10:90/EGFP plasmid, and (d) complex HBPS-N/EGFP plasmid.

nature of the carrier nanoparticles using the DNA-complexed nanoparticles HBPS-C/β-gal, HBPS-N/β-gal, HBPS-CN30:70/β-gal, and HBPS-CN10:90/β-gal. Note that the transfection efficiency with Fu-Gene6 (a commercial gene delivery vector from Roche Applied Biosystems) was considered to be 100%. Fu-Gene6 served as control for the delivery of pEGFP-N1 (1 μg) into the cells. The best transfection was obtained using the HBPS-CN30:70/β-gal complex (∼50%, see Fig. 9a). For all the measured cell lines, it is worth noting that the transfection efficiency of HBPS-C is always very low, below 5%, due to the poor coulombic interactions between nanoparticle and DNA. It is clear that the ratio of anion and cation, fully covering the nanoparticle surface, plays a key role for the gene delivery as mentioned above. Thus, even though the cationic HBPS nanoparticles provide genetic molecule delivery, HBPS-CN30:70 would be much more applicable for *in vitro* studies where efficient gene transfection is essential.

4. Conclusions

We synthesized novel HBPS materials and successfully prepared nanoparticle formulations of these polymers by exploiting specific interactions between the hydrophilic end groups (e.g. –COOH and $-N^{+}(CH_3)_3I^{-}$) and the aqueous medium. Efficient encapsulation of the hydrophobic dyes inside these HBPS nanoparticles was also achieved. Our experimental results demonstrate that the HBPS nanoparticles are useful fluorescent nanoprobes for bioimaging applications as well as suitable vehicles for nonviral gene delivery. The importance of controlling the ζ potential (surface charges) of the nanoparticles for efficient cellular uptake was demonstrated using different nanoparticle composites with widely varying ζ potential values. The finely controlled cellular-uptake properties of these nanoparticles (achieved by simply changing the terminal groups in HBPS) were also confirmed. We demonstrated successful *in vitro* delivery of pDNA-encoding proteins such as eGFP and β-gal (monitored either by confocal microscopy or by spectrophotometry) into tumor cell lines such as Cos-7 and MCF-7 using these newly synthesized HBPS nanoparticles.

Acknowledgments

This research was supported by the John R. Oishei Foundation, the Korea Science and Engineering Foundation (KOSEF-ERC Program; R11-200-050-01002) and the Basic Research Fund of Hannam University.

References

Afanasyeva, N.I., Bruch, R.F., 1999. Biocompatibility of polymer surfaces interacting with living tissue. Surf. Interface Anal. 27, 204.
Albota, M.A., Xu, C., Webb, W.W., 1998. Two-photon fluorescence excitation cross sections of biomolecular probes from 690 to 960 nm. Appl. Opt. 37, 7352–7356.
Benns, J.M., Choi, J.S., Mahato, R.I., Park, J.S., Kim, S.W., 2000. pH-sensitive cationic polymer gene delivery vehicle: N-Ac-poly(L-histidine)-graft-poly(L-lysine) comb shaped polymer. Bioconjug. Chem. 11, 637–645.
Boussif, O., Lezoualc'h, F., Zanta, M.A., Mergny, M.D., Scherman, D., Demeneix, B., Behr, J.P., 1995. A versatile vector for gene and oligonucleotide transfer into cells in culture and in vivo: polyethylenimine. Proc. Natl. Acad. Sci. U.S.A. 92, 7297–7301.
Campeau, P., Chapdelaine, P., Seigneurin-Venin, S.B.M., Tremblay, J.P., 2001. Transfection of large plasmids in primary human myoblasts. Gene Therapy 8, 1387–1394.
Cho, N.S., Hwang, D.H., Jung, B.J., Lim, E., Lee, J., Shim, H.K., 2004. Synthesis, characterization, and electroluminescence of new conjugated polyfluorene derivatives containing various dyes as comonomers. Macromolecules 37, 5265–5273.
Clarson, S.J., Semlyen, J.A., 1993. Siloxane Polymers. Prentice Hall, Englewood Cliffs, NJ.
Das, S., Jain, T.K., Maitra, A., 2002. Inorganic–organic hybrid nanoparticles from n-octyl triethoxy silane. J. Colloid Interface Sci. 252, 82–88.
Fischer, D., Bieber, T., Li, Y., Elsässer, H.-P., Kissel, T., 1999. A novel non-viral vector for DNA delivery based on low molecular weight, branched polyethylenimine: effect of molecular weight on transfection efficiency and cytotoxicity. Pharm. Res. 16, 1273–1279.
Graf, C., Schartl, W., Fischer, K., Hugenberg, N., Schmidt, M., 1999. Dye-labeled poly(organosiloxane) microgels with core-shell architecture. Langmuir 15, 6170–6180.
Grohn, F., Kim, G., Bauer, A.J., Amis, E.J., 2001. Nanoparticle formation within dendrimer-containing polymer networks: route to new organic–inorganic hybrid materials. Macromolecules 34, 2179–2185.
Kass, R.S., Krafte, D.S., 1987. Negative surface charge density near heart calcium channels. Relevance to block by dihydropyridines. J. Gen. Physiol. 89, 629–644.
Kim, K.M., Jikei, M., Kakimoto, M., 2002a. Synthesis and properties of amphiphilic hyperbranched poly(dimethylsiloxane) possessing hydrophilic terminal group. Polymer J. 34, 755–760.
Kim, K.M., Jikei, M., Kakimoto, M.A., 2002b. Preparation and properties of novel hyperbranched poly(dimethylsiloxane)s. Polymer J. 34, 275–279.

Krebs, F.C., Spanggaard, H., 2002. An exceptional red shift of emission maxima upon fluorine substitution. J. Org. Chem. 67, 7185–7192.
Li, P., Ahrens, B., Feeder, N., Raithby, P.R., Teat, S.J., Khan, M.S., 2005. Luminescent digold ethynyl thienothiophene and dithienothiophene complexes; their synthesis and structural characterisation. Dalton Trans., 874–883.
Liu, W.G., Yao, K.D., 2002. Chitosan and its derivatives—a promising non-viral vector for gene transfection. J. Control. Rel. 83, 1–11.
Marschall, P., Malik, N., Larin, Z., 1999. Transfer of YACs up to 2.3 Mb intact into human cells with polyethylenimine. Gene Therapy 6, 1634–1637.
Midoux, P., Monsigny, M., 1999. Efficient gene transfer by histidylated polylysine/pDNA complexes. Bioconjug. Chem. 10, 406–411.
Miravet, J.F., Frechet, J.M.J., 1998. New hyperbranched poly(siloxysilanes): variation of the branching pattern and end-functionalization. Macromolecules 31, 3461–3468.
Ohara, Y., Akiba, K., Inamoto, N., 1983. Alkylation of the sulfur-containing and nitrogen-containing compounds analogous to thiazoline systems. Bull. Chem. Soc. Jpn. 56, 1508–1513.
Park, J.H., Bae, Y.H., 2003. Hydrogels based on poly(ethylene oxide) and poly(tetramethylene oxide) or poly(dimethyl siloxane). III. In vivo biocompatibility and biostability. J. Biomed. Mater. Res. 64A, 309–319.
Pistel, K.F., Bittner, B., Koll, H., Winter, G., Kissel, T., 1999. Biodegradable recombinant human erythropoietin loaded microspheres prepared from linear and star-branched block copolymers: influence of encapsulation technique and polymer composition on particle characteristics. J. Control. Rel. 59, 309–325.
Prasad, P.N., 2003. Introduction of Biophotonics. Wiley-Interscience, New Jersey.
Ramzi, A., Prager, M., Richter, D., Efstratiadis, V., Hadjichristidis, N., Young, R.N., Allgaier, J.B., 1997. Influence of polymer architecture on the formation of micelles of miktoarm star copolymers polyethylene/poly(ethylenepropylene) in the selective solvent decane. Macromolecules 30, 7171–7182.
Savin, G., Bruns, N., Thomann, Y., Tiller, J.C., 2005. Nanophase separated amphiphilic microbeads. Macromolecules 38, 7536–7539.
Si, Q.-F., Wang, X., Fan, X.-D., Wang, S.-J., 2005. Synthesis and characterization of ultraviolet-curable hyperbranched poly(siloxysilane)s. J. Polymer Sci. A: Polymer Chem. 43, 1883–1894.
Strehmel, B., Sarker, A.M., Detert, H., 2003. The influence of sigma and pi acceptors on two-photon absorption and solvatochromism of dipolar and quadrupolar unsaturated organic compounds. ChemPhysChem 4, 249–259.
Suh, S.C., Suh, M.C., Shim, S.C., 1999. Photoconductivity of 3,5-dinitrobenzoate of poly[1-phenyl-1-penten-3-yn-5-ol] (DN-PPPYO) blended with poly[4-(*p*-*N*,*N*-diphenylaminophenyl)-1-phenyl-1-buten-3-yne] (PPAPBEY) as a hole transporting polymer. Macromol. Chem. Phys. 200, 1991–1997.
Tew, G.N., Pralle, M.U., Stupp, S.I., 2000. Supramolecular materials with electroactive chemical functions. Angew. Chem. Int. Ed. 39, 517–521.
Thanou, M., Florea, B.I., Geldof, M., Junginger, H.E., Borchard, G., 2002. Quaternized chitosan oligomers as novel gene delivery vectors in epithelial cell lines. Biomaterials 23, 153–159.
Tian, H.Y., Deng, C., Lin, H., Sun, J.R., Deng, M.X., Chen, X.S., Jing, X.B., 2005. Biodegradable cationic PEG-PEI-PBLG hyperbranched block copolymer: synthesis and micelle characterization. Biomaterials 26, 4209–4217.
Wetering, P.V.D., Schuurmans-Nieuwenbroek, N.M.E., Hennink, W.E., Storm, G., 1999. Comparative transfection studies of human ovarian carcinoma cells *in vitro*, *ex vivo* and *in vivo* with poly(2-(dimethylamino)ethyl methacrylate)-based polyplexes. J. Gene Med. 1, 156–165.
Xu, C., Webb, W.W., 1996. Measurement of two-photon excitation cross sections of molecular fluorophores with data from 690 to 1050 nm. J. Opt. Soc. Am. B: Opt. Phys. 13, 481–491.
Xu, Y., Szoka, F.C., 1996. Mechanism of DNA release from cationic liposome/DNA complexes used in cell transfection. Biochemistry 35, 5616–5623.